

The role of spin-orbit interaction in low thermal conductivity of Mg_3Bi_2

Nguyen Tuan Hung^{1, a)}

Frontier Research Institute for Interdisciplinary Sciences, Tohoku University, Sendai 980-8578, Japan

(Dated: 24 October 2023)

Three-dimensional layered Mg_3Bi_2 has emerged as thermoelectric material due to its high cooling performance at ambient temperature, which benefits from its low lattice thermal conductivity and semimetal character. However, the semimetal character of Mg_3Bi_2 is sensitive to spin-orbit coupling (SOC). Thus, the underlying origin of low lattice thermal conductivity needs to be clarified in the presence of the SOC. In this work, the first-principles calculations within the two-channel model are employed to investigate the effects of the SOC on the phonon-phonon scattering on the phonon transport of Mg_3Bi_2 . Our results show that the SOC strongly reduces the lattice thermal conductivity (up to $\sim 35\%$). This reduction originates from the influence of the SOC on the transverse acoustic modes involving interlayer shearing, leading to weak interlayer bonding and enhancement anharmonicity around 50 cm^{-1} . Our results clarify the mechanism of low thermal conductivity in Mg_3Bi_2 and support the design of Mg_3Bi_2 -based materials for thermoelectric applications.

The demand for green energy with net-zero gas emissions requires the development of sustainable energy-related technologies, in which thermoelectricity is one of the promising technologies that can convert heat energy into electrical energy without gas emissions. A thermoelectric (TE) device is mainly fabricated from TE material, which takes nearly one-third of the total cost of the device¹. Some of the best TE materials are Bi_2Te_3 , PbTe , and their related alloys, which were discovered around the 1950s and used as commercial TE materials^{2,3}. However, these materials are limited for wide applications due to the rare and expensive of the Te element. Therefore, during the past decade, there have been significant efforts to search for non-Te materials, such as $\alpha\text{-MgAgSb}$ ⁴, Mg_3Bi_2 ⁵⁻⁸, Bi_2Se_3 ⁹, and SnSe ¹⁰ crystals. Among them, Mg_3Bi_2 crystal is an interesting material to study the fundamental transport properties since it shows not only a high cooling performance with a large temperature difference of $\sim 91\text{ kelvin}$ ⁵ but also topological character^{11,12}.

In previous work¹², we showed that a spinless Mg_3Bi_2 could be a type-II nodal line semimetal, in which the conduction and valence bands intersect in the form of a line (called the nodal line)¹³. This feature leads to van Hove singularities near the nodal line energy and enhances the TE power factor¹². However, the nodal line character of Mg_3Bi_2 is suppressed by the spin-orbit coupling (SOC), which often happens with the Bi element. By considering the SOC, Mg_3Bi_2 becomes a normal semimetal with a tiny band gap. Then, the electronic transport properties change significantly because of the missing van Hove singularities¹². On the other hand, the SOC also can affect the thermal conductivity of the materials. Tian *et al.*¹⁴ have reported that the phonon lifetimes (or anharmonicity) of PbSe and PbTe are larger with the SOC, which leads to twice larger thermal conductivity with the SOC than that without the SOC at room temperature. Wu *et al.*¹⁵ also showed that the SOC leads to enhanced lattice

thermal conductivity of SnSe (up to $\sim 60\%$) compared without the SOC. On the other hand, Li *et al.*¹⁶ showed that the SOC does not affect the lattice thermal conductivity of Mg_2Si and Mg_2Sn due to the relatively small discrepancies between their calculations and the experimental data. These studies suggest that the SOC will play an essential role in the thermal transport in Mg_3Bi_2 . The previous reports^{17,18} focus only on the thermal properties of Mg_3Bi_2 without SOC. Thus, the role of the SOC in the low thermal conductivity of Mg_3Bi_2 still needs to be clarified to better understand the thermoelectric properties of Mg_3Bi_2 . It is noted that we can not suppress the intrinsic spin-orbit interaction in the materials. Thus, it is difficult to observe the effect of SOC on the lattice thermal conductivity by experiment. In this situation, a theoretical calculation needs to be performed first to investigate the lattice thermal conductivity of Mg_3Bi_2 with both cases of the SOC and without SOC.

In this Letter, we investigate the lattice thermal properties of Mg_3Bi_2 with and without SOC to clarify the influence of the SOC on phonon dispersion and lattice thermal conductivity, κ_l . By using the phonon Boltzmann transport with first-principle calculations, we found that the SOC reduces κ_l by about 35%, while it was reported to enhance κ_l of PbTe , PbSe , and SnSe ^{14,15}. Furthermore, the first-principle calculations within the phonon-phonon interaction underestimate κ_l compared with experimental data. Thus, we applied the two-channel model for κ_l , which accounts for the correction term by the Cahill-Watson-Pohl (CWP) formula¹⁹.

The phonon dispersion is calculated by the density-functional-perturbation theory (DFPT) with the Quantum ESPRESSO package²¹⁻²³. The fully-relativistic and scalar-relativistic ultra-soft pseudopotentials with the Perdew-Burke-Ernzerhof (PBE) functional²⁴ use for the calculations with the SOC and without the SOC, respectively. All positions of the atoms and lattice constants are optimized by the BFGS quasi-newton algorithm²³, in which the convergence values for the forces and stress components are 0.0001 Ry/a.u.^3 and 0.005 GPa , respec-

^{a)}Electronic mail: nguyen.tuan.hung.e4@tohoku.ac.jp

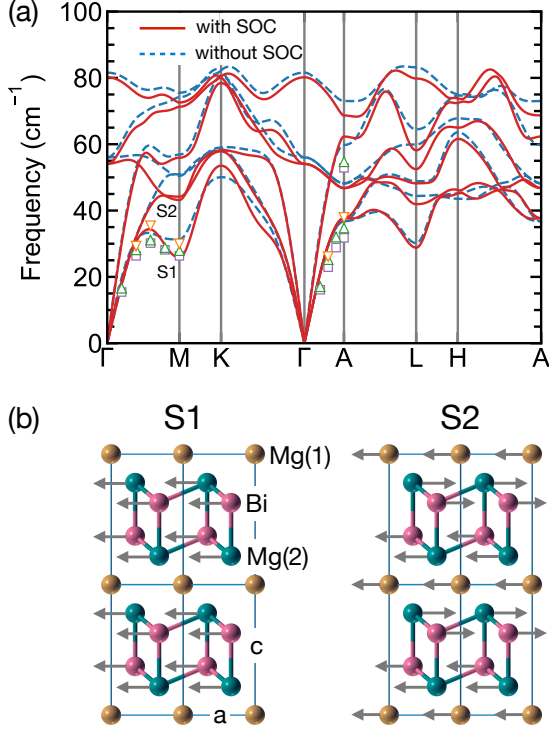


FIG. 1. (a) Phonon dispersions of Mg_3Bi_2 along the high-symmetry points in the low-frequency regime with SOC (red solid line) and without SOC (blue dashed line). The symbols represent experimental data by inelastic x-ray scattering measurements²⁰, in which ∇ , Δ , and \square markers correspond to the phonon frequencies at 80, 300, and 600 K. (b) Atomic displacements of Mg_3Sb_2 correspond to the transverse acoustic phonon modes S1 $\sim 30 \text{ cm}^{-1}$ and S2 $\sim 50 \text{ cm}^{-1}$ at the M point, which are related to the shearing modes between the Bi-Mg(2) and Mg(1) layers.

tively. The obtained lattice constants of Mg_3Bi_2 are $a = b = 4.683 \text{ \AA}$ and $c = 7.396 \text{ \AA}$, which are consistent with the previous works^{12,17}. Cutoff energy of 60 Ry, \mathbf{k} -points mesh of $10 \times 10 \times 6$, and \mathbf{q} -points mesh of $5 \times 5 \times 3$ for all calculations are selected based on the convergence test.

In Fig. 1(a), we show the phonon dispersions of Mg_3Bi_2 with the SOC (solid line) and without SOC (dashed line). Only the low-frequency regime is plotted to see the difference between the solid and dashed lines easily. We noted that the high-frequency regime above the phonon band gap could contribute less than 10% to the total thermal conductivity²⁵. The phonon dispersions reproduce the inelastic x-ray scattering (IXS) spectra²⁰, in which the case of the SOC shows a better fitting with the experimental data for the soft phonon S1 around 26 cm^{-1} at the M point. The main difference between the phonon frequency with the SOC and without the SOC is found at S1 ($\sim 5 \text{ cm}^{-1}$) and S2 ($\sim 8 \text{ cm}^{-1}$) at the M point, as shown in Fig. 1(a). The S1 and S2 phonon modes are the interlayer shearing modes in the Mg_3Bi_2

TABLE I. Bulk B , shear G , and Young E modulus (GPa), Poisson ratio r , and longitudinal v_l and transverse sound velocities v_t (m/s) of Mg_3Bi_2 .

Mg_3Bi_2	B	G	E	r	v_l	v_t
With SOC	31.81	16.44	42.07	0.28	3086.99	1707.55
Without SOC	35.44	18.29	46.81	0.28	3247.72	1795.77

with $P\bar{3}m1$ space group^{18,20}, as shown in Fig. 1(b). The Mg_3Bi_2 structures consist of alternating $[\text{Mg}(2)_2\text{Bi}_2]$ and $[\text{Mg}(1)]$ atom layers. We thus expect weak bonding between $[\text{Mg}(2)_2\text{Bi}_2]$ and $[\text{Mg}(1)]$ layers, resulting in a small shear strength. Here, we calculate the elastic modulus, including the bulk B , Young E , and shear G modulus, using the Voigt-Reuss-Hill approximation^{26,27} with the Thermo_pw code²⁸. The obtained results for the cases with and without the SOC are listed in Table I, which are consistent with the experiment data ($B = 38.39 \text{ GPa}$, $G = 13.39 \text{ GPa}$, and $E = 35.98 \text{ GPa}$ using resonant ultrasound spectroscopy¹⁸). The shear modulus of Mg_3Bi_2 is much softer than compounds with similar structures, such as CaMg_2As_2 , YbMg_2Sb_2 or BaMg_2P_2 ¹⁸, resulting in soft phonon modes of S1 and S2. Another soft phonon mode related to the interlayer shearing is found around 30 cm^{-1} at the L point, as shown in Fig. 1(b). However, the SOC does not affect this phonon mode.

In order to investigate the effect of the SOC on the lattice thermal conductivity κ_l of Mg_3Bi_2 , we calculate the two-channel model²⁹⁻³¹, which is defined as follows

$$\kappa_l = \kappa_{\text{ph}} + \kappa_{\text{diff}}, \quad (1)$$

where κ_{ph} is the phonon channel, which is defined by³²

$$\kappa_{\text{ph}} = \frac{1}{N_{\mathbf{q}}V} \sum_{\nu\mathbf{q}} \hbar\omega_{\nu\mathbf{q}} v_{\nu\mathbf{q}}^2 \tau_{\nu\mathbf{q}} \frac{\partial n_{\nu\mathbf{q}}}{\partial T}, \quad (2)$$

where $N_{\mathbf{q}}$ is the number of \mathbf{q} points and V is the volume of the unit cell. $\omega_{\nu\mathbf{q}}$, $v_{\nu\mathbf{q}}$, and $\tau_{\nu\mathbf{q}}$ is the phonon frequency, the phonon group velocity, and the phonon lifetime of the phonon mode ν at \mathbf{q} vector, respectively. $n_{\nu\mathbf{q}} = (e^{\hbar\omega_{\nu\mathbf{q}}/k_B T} - 1)^{-1}$ is the Bose-Einstein distribution function. Here, κ_{ph} and $\tau_{\nu\mathbf{q}}$ are calculated by solving the phonon Boltzmann transport equation, as implemented in the ShengBTE code³³ using $16 \times 16 \times 16$ integration meshes, based on the second-order force constants calculated the DFPT^{21,22} and third-order force constants calculated with a $3 \times 3 \times 3$ supercell and up to the five-nearest neighbors using thirdorder.py³³. κ_{diff} is the diffusion channel in the disordered crystal, which is described by the Cahill-Watson-Pohl (CWP) model as¹⁹

$$\kappa_{\text{diff}} = \left(\frac{\pi}{6}\right)^{1/3} k_B \rho^{2/3} \sum_i v_i \left(\frac{T}{\theta_i}\right)^2 \int_0^{\theta_i/T} \frac{x^3 e^x}{(e^x - 1)^2} dx, \quad (3)$$

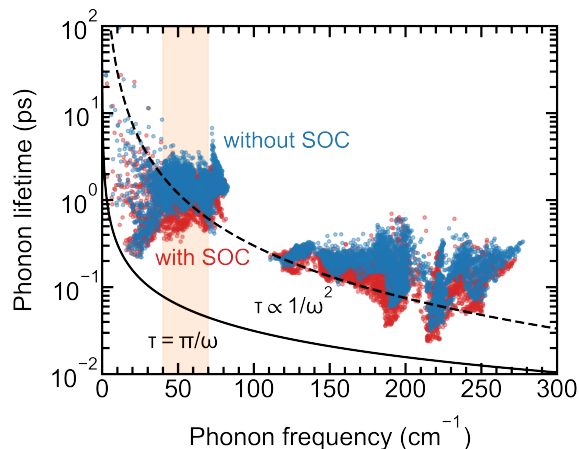


FIG. 2. Phonon lifetime τ of Mg_3Bi_2 at room temperature $T = 300$ K is plotted as a function of phonon frequency ω with SOC (red dots) and without SOC (blue dots). The black solid and dashed curves give the minimum lifetime $\tau = \pi/\omega$ from the CWP formula and $\tau \propto 1/\omega^2$ from the Umklapp scattering, respectively.

where ρ is the number density of atoms, x is the dimensionless integration variable, $\theta_i = v_i(\hbar/k_B)(6\pi^2\rho)^{1/3}$ is the Debye temperature, where v_i is the sound speed of acoustic branch i , including one longitudinal sound velocity $v_L = \sqrt{(B + 4G/3)/\rho}$ and two transverse sound velocity $v_T = \sqrt{G/\rho}$. The calculated v_L , v_T , B and G are given in Table I.

In Fig. 2, we show the phonon lifetime at $T = 300$ K of Mg_3Bi_2 with and without the SOC. The effect of the SOC on the phonon lifetime is considered only for κ_{ph} , in which the phonons frequencies below $\omega < 80$ cm^{-1} mainly dominate on κ_{ph} due to the strong frequency dependence of the Umklapp scattering ($\tau \propto 1/\omega^2$)³². For $80 < \omega < 110$ cm^{-1} , there is no phonon lifetime because of the phonon band-gap region. For $\omega > 110$ cm^{-1} , the average value of phonon lifetime is about 0.1 ps, which is one order of magnitude smaller than that for $\omega < 80$ cm^{-1} (~ 1 ps). Thus, the contribution of the SOC to κ_{ph} becomes an important factor when $\omega < 80$ cm^{-1} . In particular, the SOC leads to a reduction in the phonon lifetime around 50 cm^{-1} , which corresponds to the interlayer shearing mode S2, as shown in Fig. 1(b). We note that the high anharmonicity (i.e., low phonon lifetime) is also found at $\omega = 30$ cm^{-1} . This is the contribution of both the shearing mode S1 at the M point and another shearing mode (~ 30 cm^{-1}) at the L point (see Fig. 1(a)). Since the SOC does not affect the shearing mode at the L point, the phonon lifetime with $\omega < 30$ cm^{-1} does not change significantly with the presence of the SOC. Besides that, the SOC also does not affect the phonon lifetime in the CWP model since the CPW model assumes that the phonon lifetime is half the period of oscillation²⁹ (i.e., $\tau = \pi/\omega$).

In Fig. 3, we show the thermal conductivity κ_l of Mg_3Bi_2 as a function of the temperature T . The ob-

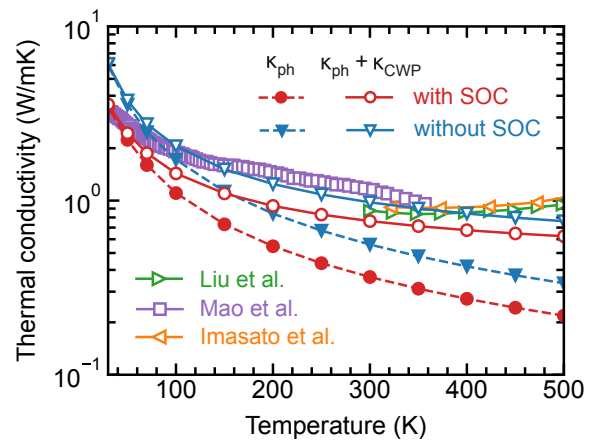


FIG. 3. Thermal conductivity of Mg_3Bi_2 with and without SOC is plotted as a function of the temperature T . Symbols \blacktriangleright , \blacksquare , and \blacktriangleleft represent the experimental data from Liu *et al.*⁸, Mao *et al.*⁵ and Imasato *et al.*⁶, respectively.

tained κ_{ph} is almost isotropic in Mg_3Bi_2 . At 300 K, $\kappa_{\text{ph}}^{xx} = \kappa_{\text{ph}}^{yy} = 0.37$; $\kappa_{\text{ph}}^{zz} = 0.36$ W/mK for the case with SOC and $\kappa_{\text{ph}}^{xx} = \kappa_{\text{ph}}^{yy} = 0.53$; $\kappa_{\text{ph}}^{zz} = 0.59$ W/mK for the case without SOC. Thus, the average value of $\kappa_{\text{ph}} = (\kappa_{\text{ph}}^{xx} + \kappa_{\text{ph}}^{yy} + \kappa_{\text{ph}}^{zz})/3$ is plotted in Fig. 3. We note that the Mg_3Bi_2 has a 3D layered structure, and it shows a two-dimensional (2D) electron character, i.e., electrons mostly move in $[\text{Mg}(2)_2\text{Bi}_2]$ layer¹². However, using quantitative analysis of chemical bonding, Zhang *et al.*³⁴ showed that the interlayer and intralayer bonds of Mg_3Bi_2 are largely ionic with partial covalent nature. Thus, Mg_3Bi_2 exhibits a nearly isotropic three-dimensional (3D) bonding network, leading to mostly isotropic κ_{ph} . Interestingly, such 2D-electron and 3D-phonon transports of Mg_3Bi_2 are opposite to 3D-electron and 2D-phonon transports of SnSe ³⁵. We can see that κ_{ph} is reduced by about 35% enhanced anharmonicity of the S2 shearing mode. Since the SOC affects the shearing modulus, it also reduces the longitudinal and transverse sound velocities (see Table I). Thus, κ_{diff} is also reduced by the SOC ($\kappa_{\text{diff}} = 0.40$ and 0.42 W/Km with SOC and with SOC, respectively). As shown in Fig. 3, κ_{ph} much lower than the experimental observation^{5,6,8} when $T > 50$ K due to neglect of the temperature-dependent anharmonic renormalization of the phonon frequencies³⁶. By using κ_{diff} to correct this term, $\kappa_{\text{ph}} + \kappa_{\text{diff}}$ can reproduce the experimental observation^{5,6,8}.

In conclusion, we have employed a two-channel model to study the effects of the SOC on the phonon dispersion, phonon anharmonicity, and thermal conductivity of Mg_3Bi_2 . Our calculations reproduce well the experimental data. The SOC not only enhances the anharmonicity of the interlayer shearing mode but also reduces the longitudinal and transverse sound velocities. Therefore, the SOC can have a considerable impact on thermal transport properties. Our calculations suggest a potential way for manipulating phonon transport by tuning the SOC.

ACKNOWLEDGMENTS

N.T.H. acknowledges financial support from the Frontier Research Institute for Interdisciplinary Sciences, Tohoku University.

REFERENCES

- ¹S. LeBlanc, S. K. Yee, M. L. Scullin, C. Dames, and K. E. Goodson, “Material and manufacturing cost considerations for thermoelectrics,” *Renew. Sustain. Energy Rev.* **32**, 313–327 (2014).
- ²H. Goldsmid and R. Douglas, “The use of semiconductors in thermoelectric refrigeration,” *Br. J. Appl. Phys.* **5**, 386 (1954).
- ³J. P. Heremans, V. Jovovic, E. S. Toberer, A. Saramat, K. Kurosaki, A. Charoenphakdee, S. Yamanaka, and G. J. Snyder, “Enhancement of thermoelectric efficiency in PbTe by distortion of the electronic density of states,” *Science* **321**, 554–557 (2008).
- ⁴H. Zhao, J. Sui, Z. Tang, Y. Lan, Q. Jie, D. Kraemer, K. McEnaney, A. Guloy, G. Chen, and Z. Ren, “High thermoelectric performance of MgAgSb-based materials,” *Nano Energy* **7**, 97–103 (2014).
- ⁵J. Mao, H. Zhu, Z. Ding, Z. Liu, G. A. Gamage, G. Chen, and Z. Ren, “High thermoelectric cooling performance of n-type Mg₃Bi₂-based materials,” *Science* **365**, 495–498 (2019).
- ⁶K. Imasato, S. D. Kang, and G. J. Snyder, “Exceptional thermoelectric performance in Mg₃Sb_{0.6}Bi_{1.4} for low-grade waste heat recovery,” *Energy Environ. Sci.* **12**, 965–971 (2019).
- ⁷X. Shi, X. Zhang, A. Ganose, J. Park, C. Sun, Z. Chen, S. Lin, W. Li, A. Jain, and Y. Pei, “Compromise between band structure and phonon scattering in efficient n-Mg₃Sb_{2-x}Bi_x thermoelectrics,” *Mater. Today Phys.* **18**, 100362 (2021).
- ⁸Z. Liu, W. Gao, H. Oshima, K. Nagase, C.-H. Lee, and T. Mori, “Maximizing the performance of n-type Mg₃Bi₂ based materials for room-temperature power generation and thermoelectric cooling,” *Nature Commun.* **13**, 1120 (2022).
- ⁹S. Wang, Y. Sun, J. Yang, B. Duan, L. Wu, W. Zhang, and J. Yang, “High thermoelectric performance in Te-free (Bi, Sb)₂Se₃ via structural transition induced band convergence and chemical bond softening,” *Energy Environ. Sci.* **9**, 3436–3447 (2016).
- ¹⁰L.-D. Zhao, S.-H. Lo, Y. Zhang, H. Sun, G. Tan, C. Uher, C. Wolverton, V. P. Dravid, and M. G. Kanatzidis, “Ultralow thermal conductivity and high thermoelectric figure of merit in SnSe crystals,” *Nature* **508**, 373–377 (2014).
- ¹¹T.-R. Chang, I. Pletikoscic, T. Kong, G. Bian, A. Huang, J. Denlinger, S. K. Kushwaha, B. Sinkovic, H.-T. Jeng, T. Valla, *et al.*, “Realization of a type-II nodal-line semimetal in Mg₃Bi₂,” *Adv. Sci.* **6**, 1800897 (2019).
- ¹²N. T. Hung, J. M. Adhidewata, A. R. Nugraha, and R. Saito, “Enhanced thermoelectric performance by van Hove singularities in the density of states of type-II nodal-line semimetals,” *Phys. Rev. B* **105**, 115142 (2022).
- ¹³B.-B. Fu, C.-J. Yi, T.-T. Zhang, M. Caputo, J.-Z. Ma, X. Gao, B. Lv, L.-Y. Kong, Y.-B. Huang, P. Richard, *et al.*, “Dirac nodal surfaces and nodal lines in zrsis,” *Sci. Adv.* **5**, eaau6459 (2019).
- ¹⁴Z. Tian, J. Garg, K. Esfarjani, T. Shiga, J. Shiomi, and G. Chen, “Phonon conduction in PbSe, PbTe, and PbTe_{1-x}Se_x from first-principles calculations,” *Phys. Rev. B* **85**, 184303 (2012).
- ¹⁵T. Wu, X. Chen, H. Xie, Z. Chen, L. Zhang, Z. Pan, and W. Zhuang, “Coupling of spin-orbit interaction with phonon anharmonicity leads to significant impact on thermoelectricity in SnSe,” *Nano Energy* **60**, 673–679 (2019).
- ¹⁶W. Li, L. Lindsay, D. A. Broido, D. A. Stewart, and N. Mingo, “Thermal conductivity of bulk and nanowire Mg₂Si_xSn_{1-x} alloys from first principles,” *Phys. Rev. B* **86**, 174307 (2012).
- ¹⁷Y. Zhu, J. Liu, B. Wei, S. Xu, Y. Song, X. Wang, T.-L. Xia, J. Chen, G. Snyder, and J. Hong, “Giant phonon anharmonicity driven by the asymmetric lone pairs in Mg₃Bi₂,” *Mater. Today Phys.* **27**, 100791 (2022).
- ¹⁸W. Peng, G. Petretto, G.-M. Rignanese, G. Hautier, and A. Zevkink, “An unlikely route to low lattice thermal conductivity: small atoms in a simple layered structure,” *Joule* **2**, 1879–1893 (2018).
- ¹⁹D. G. Cahill, S. K. Watson, and R. O. Pohl, “Lower limit to the thermal conductivity of disordered crystals,” *Physical Review B* **46**, 6131 (1992).
- ²⁰J. Ding, T. Lanigan-Atkins, M. Calderón-Cueva, A. Banerjee, D. L. Abernathy, A. Said, A. Zevkink, and O. Delaire, “Soft anharmonic phonons and ultralow thermal conductivity in Mg₃(Sb,Bi)₂ thermoelectrics,” *Sci. Adv.* **7**, eabg1449 (2021).
- ²¹S. Baroni, S. De Gironcoli, A. Dal Corso, and P. Giannozzi, “Phonons and related crystal properties from density-functional perturbation theory,” *Rev. Mod. Phys.* **73**, 515 (2001).
- ²²P. Giannozzi, S. Baroni, N. Bonini, M. Calandra, R. Car, C. Cavazzoni, D. Ceresoli, G. L. Chiarotti, M. Cococcioni, I. Dabo, *et al.*, “QUANTUM ESPRESSO: a modular and open-source software project for quantum simulations of materials,” *J. Phys. Condens. Matter* **21**, 395502 (2009).
- ²³N. T. Hung, A. R. Nugraha, and R. Saito, *Quantum ESPRESSO course for solid-state physics* (Jenny Stanford Publishing, New York, 2022).
- ²⁴J. P. Perdew, K. Burke, and M. Ernzerhof, “Generalized gradient approximation made simple,” *Phys. Rev. Lett.* **77**, 3865 (1996).
- ²⁵B. Dong, Z. Wang, N. T. Hung, A. R. Oganov, T. Yang, R. Saito, and Z. Zhang, “New two-dimensional phase of tin chalcogenides: Candidates for high-performance thermoelectric materials,” *Phys. Rev. Mater.* **3**, 013405 (2019).
- ²⁶O. L. Anderson, “A simplified method for calculating the Debye temperature from elastic constants,” *J. Phys. Chem. Solids* **24**, 909–917 (1963).
- ²⁷N. T. Hung, A. R. Nugraha, and R. Saito, “Three-dimensional carbon Archimedean lattices for high-performance electromechanical actuators,” *Carbon* **125**, 472–479 (2017).
- ²⁸A. Dal Corso, “Elastic constants of beryllium: a first-principles investigation,” *J. Phys. Condens. Matter* **28**, 075401 (2016).
- ²⁹S. Mukhopadhyay, D. S. Parker, B. C. Sales, A. A. Puretzky, M. A. McGuire, and L. Lindsay, “Two-channel model for ultralow thermal conductivity of crystalline Tl₃VSe₄,” *Science* **360**, 1455–1458 (2018).
- ³⁰P.-H. Du, C. Zhang, T. Li, and Q. Sun, “Low lattice thermal conductivity with two-channel thermal transport in the superatomic crystal PH₄AlBr₄,” *Phys. Rev. B* **107**, 155204 (2023).
- ³¹Y. Luo, X. Yang, T. Feng, J. Wang, and X. Ruan, “Vibrational hierarchy leads to dual-phonon transport in low thermal conductivity crystals,” *Nat. Commun.* **11**, 2554 (2020).
- ³²N. T. Hung, A. R. Nugraha, and R. Saito, “Designing high-performance thermoelectrics in two-dimensional tetradymites,” *Nano Energy* **58**, 743–749 (2019).
- ³³W. Li, J. Carrete, N. A. Katcho, and N. Mingo, “ShengBTE: A solver of the Boltzmann transport equation for phonons,” *Comp. Phys. Commun.* **185**, 1747–1758 (2014).
- ³⁴J. Zhang, L. Song, M. Sist, K. Tolborg, and B. B. Iversen, “Chemical bonding origin of the unexpected isotropic physical properties in thermoelectric Mg₃Sb₂ and related materials,” *Nat. Commun.* **9**, 4716 (2018).
- ³⁵C. Chang, M. Wu, D. He, Y. Pei, C.-F. Wu, X. Wu, H. Yu, F. Zhu, K. Wang, Y. Chen, *et al.*, “3D charge and 2D phonon transports leading to high out-of-plane ZT in n-type SnSe crystals,” *Science* **360**, 778–783 (2018).
- ³⁶Y. Xia, K. Pal, J. He, V. Ozoliņš, and C. Wolverton, “Particle-like phonon propagation dominates ultralow lattice thermal conductivity in crystalline Tl₃VSe₄,” *Phys. Rev. Lett.* **124**, 065901 (2020).